JMEPEG (2006) 15:53-58
DOI: 10.1361/105994905X64530

1059-9495/$19.00

Corrosion Behavior of Engineering Alloys in Synthetic Wastewater

R. Sandoval-Jabalera, E. Arias-del Campo, J.G. Chacón-Nava, J.M. Malo-Tamayo, J.L. Mora-Mendoza, and A. Martínez-Villafañe

(Submitted March 1, 2005; in revised form July 21, 2005)

The corrosion behavior of 1018, 410, and 800 steels exposed to synthetic wastewater have been studied using linear polarization resistance, cyclic potentiodynamic curves (CPCs), electrochemical noise (EN), and electrochemical impedance spectroscopy (EIS) tests. The conditions were: a biochemical oxygen demand of 776 ppm; a chemical oxygen demand of 1293 ppm; a pH of 8; and a cell temperature of 25 °C. From the CPC and EN results, no localized corrosion was found for the stainless steels. However, small indications of a possible localized corrosion process were detected for the 1018 steel. The EIS results revealed that different corrosion mechanisms occurred in the carbon steel compared with the stainless steels. The results show that the corrosion mechanism strongly depends on the type of steel. Overall, the 1018 steel exhibited the highest corrosion rate, followed by the 410 alloy. The highest corrosion resistance was achieved by the 800 alloy. In addition, scanning electron microscopy analyses were carried out to explain the experimental findings.

Keywords carbon steel, corrosion behavior, electrochemical techniques, stainless steels, synthetic wastewater

1. Introduction

Corrosion is a heterogeneous process involving reactions between a metal and its environment. As corrosion reactions involve the transfer of electrons, corrosion is an electrochemical process of oxidation and reduction reactions (Ref 1). Electrochemical measurements are now widely used in most fields of corrosion research (Ref 2). Detailed reviews are available on the application of electrochemical techniques such as linear polarization resistance (LPR) (Ref 3-5), polarization curves (Tafel slopes) (Ref 6-8), electrochemical noise (EN) (Ref 9-15), and electrochemical impedance spectroscopy (EIS) (Ref 11, 16-20), among others. In wastewater systems, both metallic materials (e.g., steel, cast iron, and stainless steel) and nonmetallic materials [e.g., concrete, acrylonitrile butadiene styrene (ABS), and polyvinyl chloride (PVC)] are widely used. For such systems, various strategies that may be used to prevent or minimize corrosion are better design parameters, the modification of the environment, and the selection of construction materials (Ref 21). Also, coal tar epoxy systems applied to the interior of concrete pipes have been reported (Ref 22). Regarding metallic materials issues, some valuable work has been accomplished in the evaluation of materials performance in water systems by using various techniques. Korshin and coworkers (Ref 23) reported a study on the effect of natural organic matter in potable water on the corrosion of leaded brass using x-ray photoemission spectroscopy and surface ion mass-spectroscopy techniques. Iversen (Ref 24) studied the microbial corrosion of AISI 304 and AISI 316 stainless steels in wastewater treatment plants with the open circuit potential technique. Tuthill (Ref 25) reported polarization curves for as-welded 304L (with heat tint) and as-welded and pickled (heat scale removed) conditions on the corrosion behavior of austenitic stainless steels in wastewater environments.

Thus, the goal of the present work was to ascertain the corrosion behavior of three alloys with different chromium content exposed into simulated synthetic wastewater by using various electrochemical techniques.

R. Sandoval-Jabalera, E. Arias-del Campo, J.G. Chacón-Nava, and **A. Martínez-Villafañe,** Advanced Materials Research Centre, Division of Materials Deterioration and Structural Integrity, Miguel de Cervantes 120, Complejo Ind. Chihuahua, C.P. 31109, Chihuahua, Chihuahua, México; **J.M. Malo-Tamayo,** Electrical Research Institute, Mechanical Systems Division, Avenida Reforma, C.P. 62490, Cuernavaca, Morales, México; and **J.L. Mora-Mendoza,** Petroleos Mexicanos, Pemex Gas Petroquimica Basica, Avenida Marina Nacional 329, Col. Huisquilucan, C.P. 11311, México, D.F. México. Contact e-mail: raul.sandoval@cimav.edu.mx.

2. Experimental Procedures

The materials used were carbon steel 1018, a martensitic 410 stainless steel, and an austenitic high alloy 800 used typically in high-temperature applications. Their chemical compositions are shown in Table 1.

2.1 Materials Preparation

Specimens from the various alloys (working electrodes) were cut from rods into coupons. Specimen dimensions were: 1.27 cm in diameter × 2 cm in length for the 1018 steel and the 800 alloy; and 0.316 cm in diameter × 2 cm in length for the 410 steel. The specimens were mounted in epoxy resin. After mounting, each specimen was polished with 1200-grit SiC paper, washed with distilled water, degreased with acetone, and dried prior to the tests. Synthetic wastewater was prepared using 5 g of ground organic matter dissolved in 1 L of potable water. Table 2 shows the characterization analysis of synthetic wastewater.

2.2 Electrochemical Techniques

Electrochemical experiments were carried out using an ACM Gill 8 (Applied Corrosion Monitoring Instruments, Cum-

Table 1 Chemical composition of the alloys used (wt.%)

UNS number	Name	Fe	C	Mn	S	P	Cr	Ni	Si	Cu	Mo	Ti	Al
G10180	1018	Balance	0.15-0.20	0.60-0.90	0.05	0.04	…	…	…	…	…	…	…
S41000	410	Balance	0.15	1	0.03	0.04	11-13	…	1.0	…	…	…	…
N08800	800	Balance	0.1	1.5	0.015	0.015	19-23	30-35	1.0	0.75	…	0.6	0.6

Table 2 Chemical characterization of synthetic wastewater (the matrix of the solution was potable water)

Parameter	Values
Biochemical oxygen demand	776 ppm
Chemical oxygen demand	1293 ppm
Temperature	21 °C
pH	8
Calcium	38 ppm
Alkalinity (HCO_3)	57 ppm
Chloride	12 ppm
Sulfate	48 ppm

bria, UK) internal potentiostat, zero resistance ammeter (ZRA), frequency response analyzer, and galvanostat controlled by a personal computer. All the potentials were measured versus a saturated calomel electrode (SCE) as the reference electrode. The counterelectrode was a platinum foil. The LPR measurements were carried out by applying a small sweep from –20 to +20 mV around the rest potential at a scan rate of 1.5 mV/s.

From the LPR data, the corrosion rates were calculated in terms of the corrosion current density, i_{corr}, using the equation of Stearn and Geary (Ref 26). The i_{corr} value was calculated as follows:

$$i_{corr} = 26/R_p \quad \text{(Eq 1)}$$

where 26 is a Tafel constant value given by the software used and R_p is the polarization resistance. The corrosion rates, reported in millimeters per year, were calculated according to Faraday's law. All tests started after 1 h of exposure.

Cyclic polarization curves (CPC) were included in this work to evaluate the conditions of passivity and the tendency of the metals to experience local pitting (Ref 27). In this case, the applied potential varied from –1 V to +1 V at a scan rate of 90 mV/min. The EN measurements were based on the ASTM standard (Ref 28). To detect the potential and current noise, an arrangement of two nominally identical working electrodes were used. To obtain potential noise data, the potential of one electrode was measured relative to a reference electrode (SCE) by using a high-resolution voltmeter. The current noise measurements were performed using a ZRA connected to a personal computer. The current noise was measured as the galvanic coupling current between the two identical electrodes. The current noise and potential measurements were monitored simultaneously at a sampling interval of 1 s. For each alloy, signals were collected over a period of 1024 s. Experimental Nyquist diagrams were obtained by EIS using a small-amplitude signal [$\Delta V = 10$ mV root mean square (rms)] over a frequency range from 20 MHz to 0.01 Hz. In all cases, the experiments were carried out at room temperature (≈25 °C).

2.3 Scanning Electron Microscopy Observations

After exposure to the environment, the morphology of the exposed surfaces was observed by conventional scanning electron microscopy (SEM).

3. Results and Discussion

3.1 Linear Polarization Resistance Tests

From the LPR tests, the E_{corr} values recorded for the 1018 steel, the 410 steel, and the 800 steel were, –272, +102, and –13.3 mV, respectively. Table 3 shows the values of polarization resistance, i_{corr}, and corrosion rates recorded for the various materials. From Table 3, it can be noted that the 1018 alloy disclosed a higher corrosion rate than those for the other alloys. Significant differences were noted among the alloys. For instance, the corrosion rate difference between the 1018 carbon steel and the 410 stainless steel were about two orders of magnitude, and in comparison with the 1018 carbon steel and the 800 stainless steel the differences were about three orders of magnitude. It is thought that the higher corrosion resistance of the stainless steels is related to their chromium content.

3.2 Cyclic Potentiodynamic Curve Tests

The results from the CPC tests (Fig. 1) indicated different behavior for the alloys. The shape of the anodic curve for the 1018 steel shows a passive behavior at approximately 130 mV. To some extent, this could be due to the formation of corrosion products on the steel surface. However, the probability of a localized attack is indicated by the hysteresis loop recorded on this steel. The pitting potential, Ep, was reached at about 600 mV. The hysteresis loop indicates a poor repassivating ability and a low protection potential, Eprot, of about 400 mV. The curves for 410 and 800 steels showed a rather different behavior. The shape of the anodic curve shows a narrow range of passivation potential, being somewhat larger for the 800 alloy (i.e., the breakdown potential for the 410 steel is about 845 mV, whereas for the 800 steel it was about 870 mV). For these materials, a hysteresis loop was not found. Instead, the curves exhibited instantaneous repassivation on the reverse scan. Very similar results have been reported using stainless steels exposed to diluted sulfuric acid at 30 °C (Ref 29). In summary, under the experimental conditions of the present work, the stainless steels used here were not susceptible to localized corrosion.

3.3 Electrochemical Noise Tests

Potential, current, and time records for the three types of steels are shown in Fig. 2, 3, and 4. The current trend of the signals was removed using the moving average removal method (Ref 30). It can be observed that the amplitude of the

voltage fluctuations are at least one order of magnitude higher for the 1018 steel compared with the 410 and 800 alloys. Also, the 1018 steel signal displays a different shape with spikes combined with low-amplitude and low-frequency fluctuations. On the other hand, the current fluctuations follow the opposite order where fluctuations are much smaller for the 410 and 800 steels than those obtained for the 1018 steel, indicating a less active interface. This is reflected in the standard deviation values of the steels shown in Table 4. These values allow the calculation of noise resistance, R_n, for each material from Eq 2:

$$R_n = \sigma_v / \sigma_i \quad \text{(Eq 2)}$$

Table 3 Polarization resistance, corrosion current density, and corrosion rates obtained from polarization resistance

Alloy	R_p, Ohm · cm^2	i_{corr}, mA/cm^2	Corrosion rate, mm/yr
1018	4.93E03	5.27E-03	2.67E-02
410	4.45E05	5.84E-05	6.44E-04
800	4.19E06	6.21E-06	6.40E-05

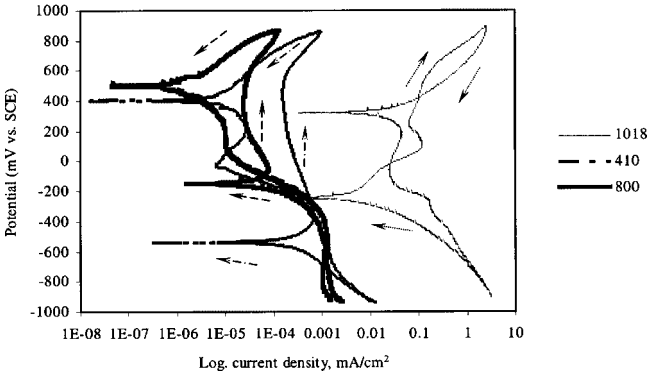

Fig. 1 Cyclic potentiodynamic curves for 1018, 410, and 800 steels

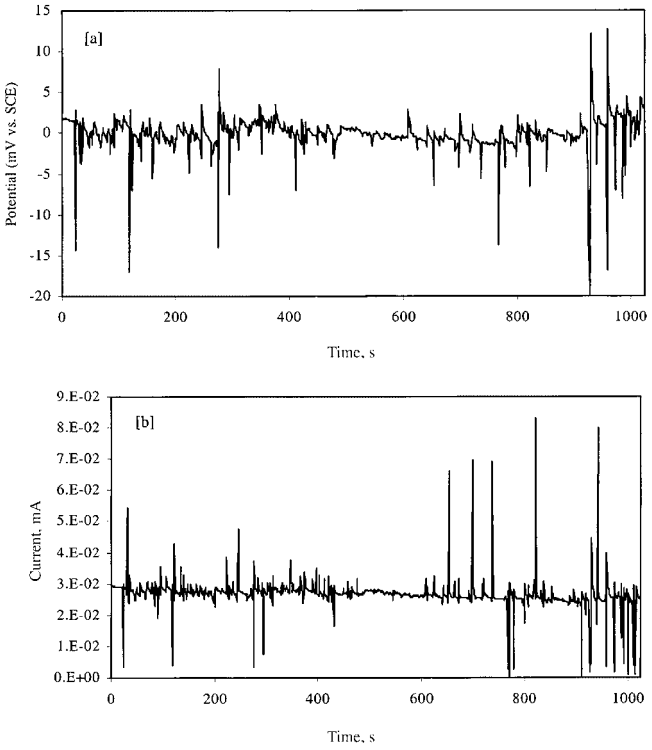

Fig. 2 (a) Potential and (b) current time records for 1018 steel in the test solution

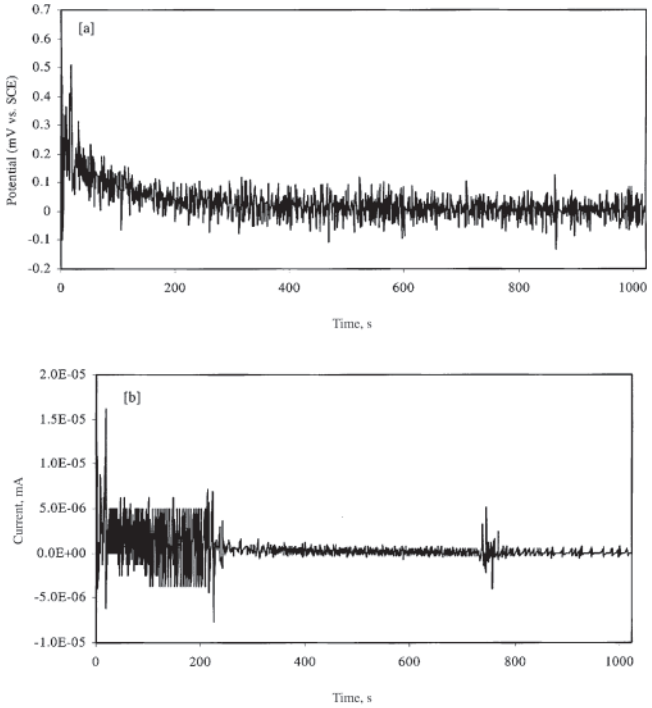

Fig. 3 (a) Potential and (b) current time records for 410 steel in the test solution

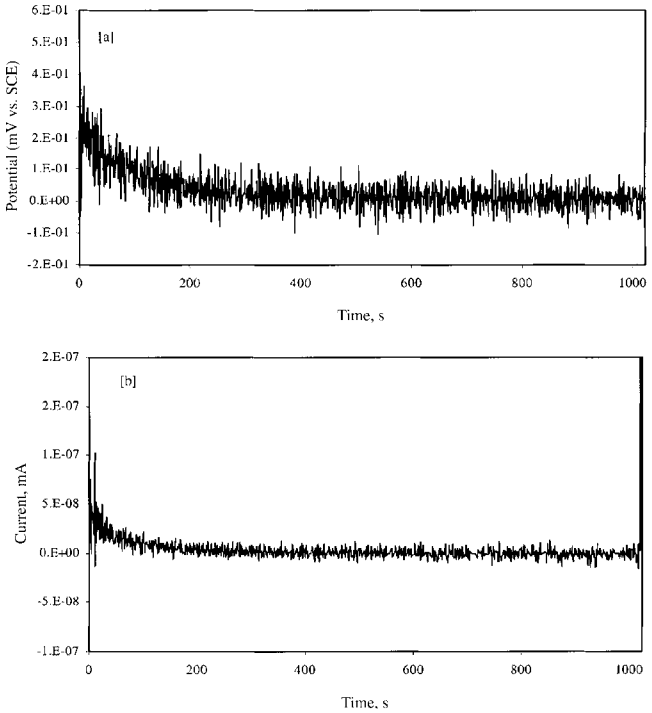

Fig. 4 (a) Potential and (b) current time records for 800 steel in the test solution

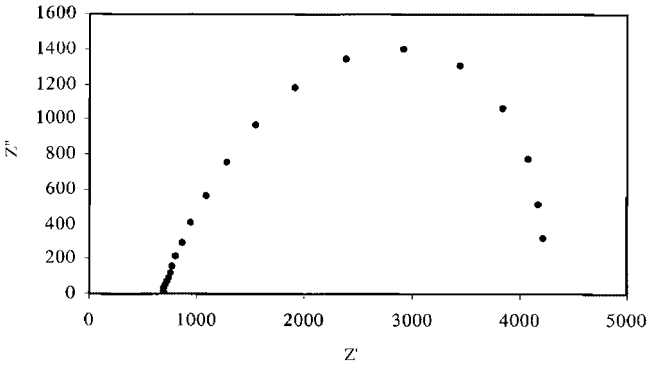

Fig. 5 Nyquist diagram for the 1018 alloy

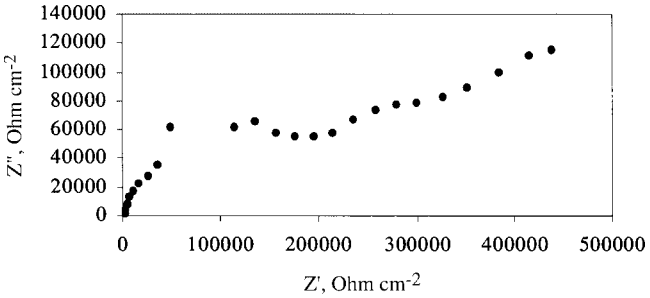

Fig. 6 Nyquist diagram for the 410 alloy

Table 4 Electrochemical noise parameters

Alloy	σ_v	σ_i	R_n	Corrosion rate, mm-y	LI	Description
1018	0.858	1.37E-03	6.25E00	2.10E-01	0.194	Uniform corrosion with localized corrosion
410	0.034	2.58E-07	1.32E05	2.1E-03	0.016	Predominant uniform corrosion
800	0.038	4.18E-09	9.13E06	2.92E-05	0.009	Predominant uniform corrosion

Table 5 Polarization resistance and corrosion current density obtained from electrochemical impedance spectroscopy

Alloy	R_p, Ohm · cm^2	i_{corr}, mA/cm^2
1018	3.55E03	7.32E-03
410	2.4E05	1.08E-04
800	3.1E05	8.38E-05

where σ_v is the standard deviation of the potential noise, and σ_i is the standard deviation of the current noise (Ref 31).

From these results, a performance order can be established in which the 1018 steel shows the lowest resistance, and therefore the highest corrosion rate, a value that is similar to that obtained using other techniques. The 410 and 800 steels follow with resistances that are several orders of magnitude higher than that of the 1018 steel. Therefore, the best corrosion rate behavior corresponds to that for the 800 steel followed by that for the 410 and 1018 steels. The prediction of corrosion rate values using EN rates are similar to those obtained by other techniques, apart from the fact that for the 800 steel smaller values were obtained.

Regarding the localized nature of the attack, the localization index, LI, is defined as:

$$LI = \sigma_i / I_{rms} \quad \text{(Eq 3)}$$

where I_{rms} is the rms value of the current noise. The LI falls in the range of 0.0 to 1. Values on the order of 0.001 indicate that uniform general corrosion is the predominant mechanism, whereas values approaching 1 indicate the predominance of a localized mechanism (Ref 32, 33). The LI was found to differentiate between low-corrosion passive behavior and localized corrosion in this environment. The 410 and 810 alloy materials can be differentiated because their values are closer to 0 and therefore indicate the predominance of uniform corrosion; in contrast, the L value for 1018 steel is higher and closer to 1, which suggests a localized contribution not found in the other steels (Table 4). This is in agreement with SEM observations of the surface morphology of the alloys.

In summary, corrosion parameters were calculated from EN measurements, particularly, noise resistance, which is related to the general corrosion rate, and the LI, which indicates the predominant corrosion attack mechanism. Differences were found for the steels that were studied.

3.4 Electrochemical Impedance Spectroscopy Tests

To obtain a better understanding of the mechanisms taking place at the specimen surface, EIS measurements at the corrosion potential were carried out under potentiostatic conditions. The Nyquist diagram obtained for the 1018 steel (Fig. 5) shows a typical Randles circuit, which is typical of an activation control process. From this diagram, Table 5 shows the estimated values for R_p, and i_{corr}, which are in good agreement with the values reported in Table 3 (i.e., the values obtained by LPR). The data agree well with the values reported for mild steel exposed in natural waters (Ref 11). The 410 alloy (Fig. 6) shows a depressed semicircle at intermediate frequencies and diffusional behavior at low frequencies, probably associated with the formation of a thin protective oxide film. In cases like this, which have been associated with passive metals, the data do not reach a low-frequency limit and show only a partial semicircle (Ref 6, 11, 34). The mechanism observed for the 800 alloy (Fig. 7) is similar to that of the 410 steel. On both stainless steels, the extrapolation of the semicircle depicted in the Nyquist diagrams gives an R_p value from which i_{corr} values can be derived in each case. Again, the values given in Table 5 are in close agreement with the values indicated in Table 3.

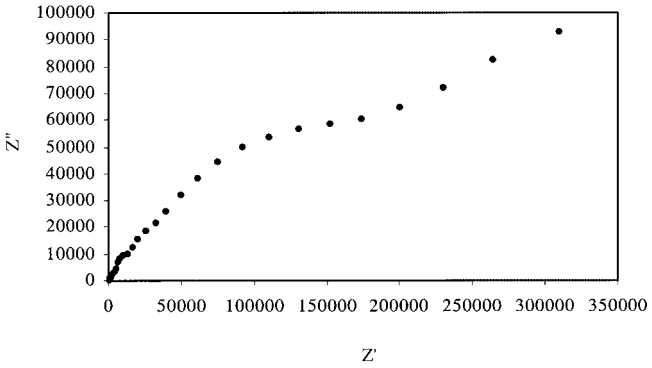

Fig. 7 Nyquist diagram for the 800 alloy

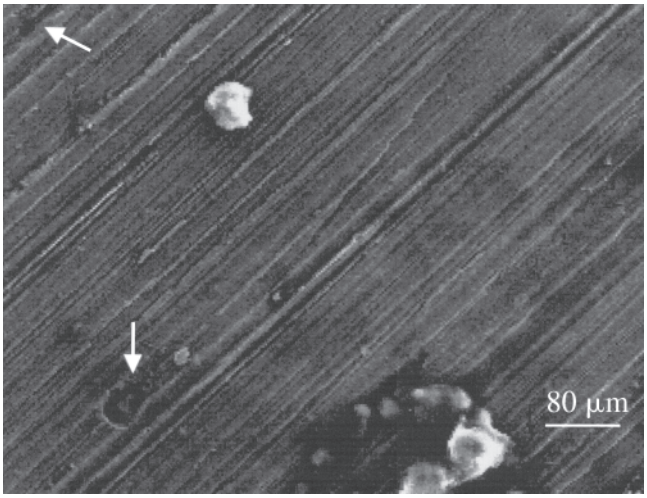

Fig. 8 An SEM image of the 1018 steel after exposure to the environment showing areas with pitting

3.5 Scanning Electron Microscopy Observations

For the 1018 steel, SEM observations on the exposed surface showed a few areas of localized corrosion as pitting, as can be seen in Fig. 8 and 9. To some extent, this confirms the CPC trend and EN results obtained for this low-alloy steel. Observations on the surfaces of the 410 steel (Fig. 10) and 800 steel (Fig. 11) still showed grinding marks from the preparation of the specimen, and evidence of pit formation was not observed on the entire exposed surface. In both cases, no localized damage could be observed. It is believed that the chromium content of these alloys might induce the formation of a protective oxide film, explaining the low corrosion rates measured on these steels.

4. Conclusions

The corrosion behavior of 1018, 410, and 800 steels exposed to synthetic wastewater was examined through various electrochemical techniques. The LPR results indicated that the 800 steel exhibited the best corrosion resistance, followed by that of the 410 steel. The highest corrosion rate was for the 1018 steel. The CPC and EN behaviors indicated that the 1018 steel is susceptible to localized corrosion in this environment. The opposite was found for the 410 and 800 alloys. For the

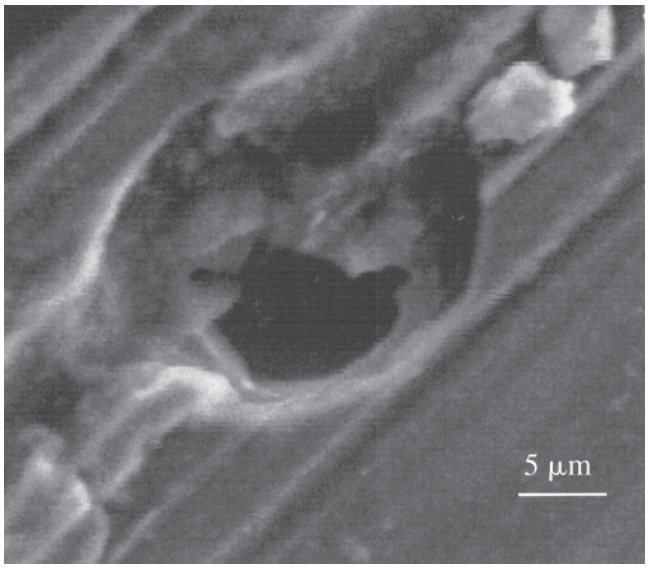

Fig. 9 An SEM image of the 1018 steel showing pitting

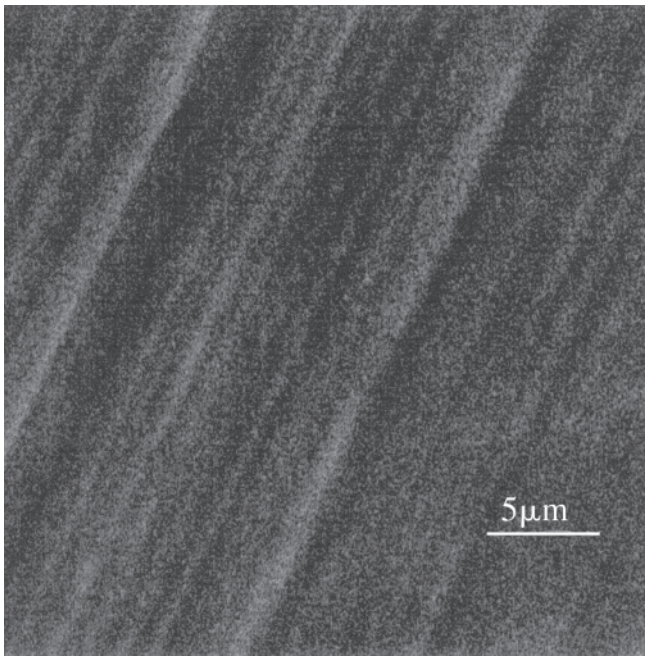

Fig. 10 An SEM image of the 410 steel after exposure to the environment showing grit lines from the initial surface preparation

1018 steel, EN measurements and analysis indicated that the predominant corrosion attack mechanism was one of uniform corrosion, with some indications of a localized corrosion process, as observed in a few areas of the exposed surface. For the stainless steels, evidence of pit formation could not be observed on the entire exposed surface. It is believed that the passive behavior shown by stainless steels is due to the formation of a protective thin oxide film on the surface of the alloy. The EIS results showed that different corrosion mechanisms occurred on the steels. The 1018 steel showed an activation mechanism, whereas the stainless steels showed a diffusion mechanism. On the whole, the electrochemical techniques used here were useful to ascertain the corrosion behavior of steels exposed to a wastewater environment.

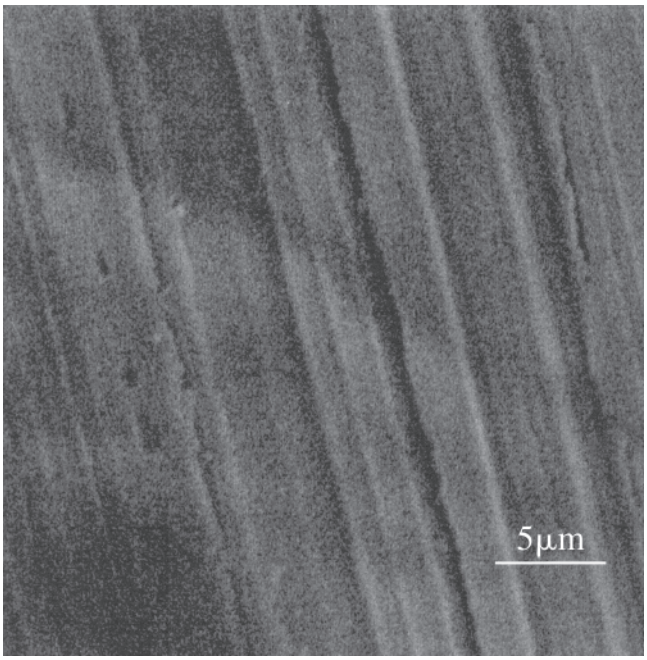

Fig. 11 An SEM image of the 800 steel after exposure to the environment showing grit lines from initial surface preparation

Acknowledgments

The authors wish to thank the support of Consejo Nacional de Ciencia y Tecnologia (National Council of Science and Technologie) (Mexico), and Prof. J. Genescá, Universidad Autonoma de Mexico (National Autonomous University of Mexico) for fruitful discussions.

References

1. B. Pesic and V.C. Storhock, "Biocorrosion of Iron with *Thiobacillus ferrooxidans:* Linear Polarization Study," Paper No. 1255, Presented at Corrosion 2001 (Houston, TX), NACE, 2001
2. B. Poulson, Electrochemical Measurements in Flowing Solutions, *Corros. Sci.,* 1983, 23, p 391-430
3. G. Rocchini, The Influence of the Ohmic Drop on the Shape of Polarization Curves, *Corros. Sci.,* 1993, 34, p 2019-2030
4. G. Rocchini, The Influence of the Potential Sweep Rate on the Computation of the Polarization Resistance, *Corros. Sci.,* 1996, 38, p 2095-2109
5. J.R. Scully, Polarization Resistance Method for Determination of Instantaneous Corrosion Rates, *Corrosion,* 2000, 56, p 199-218
6. H.W. Pickering, Characteristic Features of Alloy Polarization Curves, *Corros. Sci.,* 1983, 23, p 1107-1120
7. B.R. Pearson and P.A. Brook, The Synthesis of Electrode Polarization Curves, *Corros. Sci.,* 1991, 32, p 387-398
8. G. Rocchini, A Theoretical Study of the Influence of the Ohmic Drop on Polarization Curves, *Corros. Sci.,* 1996, 38, p 655-668
9. C. Gabrielli, F. Huet, and M. Keddam, *Corrosion,* 1992, 48, p 794-811
10. J. Uruchurtu and J.L. Dawson, Noise Analysis of Pure Aluminum Under Different Pitting Conditions, *Corrosion,* 1987, 43, p 19-26
11. J. Uruchurtu–Chavarín and J.M. Malo, Electrochemical Noise as a Powerful Electrochemical Technique for Corrosion Studies, *Res. Trends,* 1997, 2, p 49-58
12. U. Bertocci, F. Huet, B. Jaoul, and P. Rousseau, Frequency Analysis of Transients in Electrochemical Noise: Mathematical Relationships and Computer Simulations, *Corrosion,* 2000, 56, p 675-683
13. R.A. Cottis, Interpretation of Electrochemical Noise Data, *Corrosion,* 2001, 57, p 265-285
14. A. Aballe, A. Bautista, U. Bertocci, and F. Huet, Measurements of the Noise Resistance for Corrosion Applications, *Corrosion,* 2001, 57, p 35-42
15. D.A. Eden and G.P. Quirk, "Reference Electrodes in Plant Corrosion Monitoring: Who Needs Them?", Paper 1303, presented at Corrosion 2001 (Houston, TX), NACE, 2001
16. D.D. MacDonald, Some Advantages and Pitfalls of Electrochemical Impedance Spectroscopy, *Corrosion,* 1990, 46, p 229-242
17. P. Agarwal, O.C. Moghissi, M.E. Orazem, and L.H. García-Rubio, Application of Measurement Models for Analysis of Impedance Spectra, *Corrosion,* 1993, 49, p 278-289
18. J.R. Scully, D.C. Silverman, and M.W. Kending, Ed., *Electrochemical Impedance, Analysis and Interpretation,* STP 1188, ASTM, 1993
19. L. Domingues, C. Oliveira, J.C.S. Fernandes, and M.G.S. Ferreira, EIS on Plasma-Polymerized Coatings Used as Pre-Treatment of Aluminum Alloys, *Electrochim. Acta,* 2002, 47, p 2253-2258
20. M.A. González-Nuñez and J. Uruchurtu-Chavarín, "R/S Fractal Analysis of Electrochemical Noise Signals of Three Organic Coating Samples Under Corrosion Conditions," Paper C117, presented at Corrosion Science in the 21st Century (Manchester, U.K.), July 2003
21. K.B. Tator, Preventing Hydrogen Sulphide and Microbiologically Influenced Corrosion in Wastewater Facilities, *Mater. Perf.,* 2003, 42, p 32-37
22. S.H. Gebler and R.J. Detwiler, Avoiding Sewer Replacement Through Rehabilitation, *Mater. Perf.,* 2002, 41, p 32-36
23. G.V. Korshin, J.F. Ferguson, and A.N. Lancaster, Influence of Natural Organic Matter on the Corrosion of Leaded Brass in Potable Water, *Corros. Sci.,* 2000, 42, p 53-66
24. A. Iversen, Microbiologically Influenced Corrosion on Stainless Steels in Wastewater Treatment Plants: Part 1, *Br. Corros. J.,* 2001, 36, p 277-283
25. A.H. Tuthill, "Guidelines for the Use of Stainless Steel in Municipal Waste Water Treatment Plants," NIDI Technical Series No. 10076, 1995
26. M. Stearn and A.L. Geary, Electrochemical Polarization: I. A Theoretical Analysis of the Shape of Polarization Curves, 1957, 104, p 56-63
27. "Standard Practice for Conducting Cyclic Potentiodynamic Polarization Measurements for Localized Corrosion," G61-86, *Annual Book of ASTM Standards,* ASTM, 1998, p 340
28. J.R. Kearns, D.A. Eden, M.R. Yaffe, J.V. Fahley, D.L. Reichert, and D.C. Silverman, ASTM Standardization of Electrochemical Noise Measurement, *Electrochemical Noise Measurements for Corrosion Applications ASTM STP 1277,* J.R. Kearns, J.R. Scully, P.R. Roberge, D.L. Reichert, J.L. Dawson, Ed., American Society for Testing and Materials, ASTM, 1996, p 446-470
29. O.W. Siebert, Application of Rapid-Scan Potentiodynamic Polarization Technique for Corrosion Studies, *Electrochemical Techniques for Corrosion Engineering,* R. Baboian, Ed., NACE, Houston, TX, 1986, p 81-92
30. Y.J. Tan, S. Bailey, and B. Kinsella, The Monitoring of the Formation and Destruction of Corrosion Inhibitor Film Using Electrochemical Noise Analysis (ENA). *Corros. Sci.,* 1996, 38, p 1681-1695
31. A.N. Rothwell and D.A. Eden, Electrochemical Noise Data: Analysis, Interpretation, and Presentation, paper 223, presented at Corrosion 92, NACE, 1992, Houston, TX
32. S. Webster, L. Nathanson, A.G. Green, and B.V. Johnson, "The Use of Electrochemical Noise to Assess Inhibitor Film Stability," presented at Corrosion 92, Manchester, U.K., 1992
33. J. Mickalonis, R.J. Jacko, G.P. Quirk, and D.A. Eden, "The Use of Electrochemical Noise Measurements With Nuclear Waste Tanks," *Electrochemical Noise Measurements for Corrosion Applications,* ASTM STP 1277, J.R. Kearns, J.R. Scully, P.R. Roberge, D.L. Reichert, and J.L. Dawson, Ed., ASTM, 1996, p 210-213
34. K. Hladky, L.M. Callow, and J.L. Dawson. Corrosion Rates from Impedance Measurements: An Introduction, *Br. Corros. J.,* 1980, 15, p 20-25